Application of an open-loop dynamic wake model with high-frequency SCADA data

R. Braunbehrens[1], J. Schreiber[2], C. L. Bottasso[1]

[1] Wind Energy Institute, Technische Universität München, Garching bei München, Germany,
[2] Windparkanalysen und Beratung, Schreiber (WAB-S)

E-mail: robert.braunbehrens@tum.de, schreiber@wab-s.de, carlo.bottasso@tum.de

Abstract. Future wind energy control applications require surrogate flow models that can capture processes on short time scales. Dynamic extensions of wake models might be a useful low cost solution. So far, studies have tested the proposals mostly in LES or LIDAR campaigns. At the same time, readily obtainable turbine SCADA measurements are increasingly being used directly for model input or validation. Newly available high resolution recordings allow for the study of processes on shorter time scales. The present study examines the modelling capabilities of a dynamic wake model by utilizing high frequency SCADA data. Therefore, the data is first analyzed for cross-correlation and time delays. Secondly, the dynamic wake model, initialized with SCADA measurements, is used to predict a two turbine wake interaction. An offline tuning algorithm is used to adapt the model for the shorter time scales.

1. Introduction

Modern wind energy control applications aim to overcome the conventional, greedy power generation [17, 32]. These new regulation strategies propose to unlock untapped potential in wind farm operation. One of the mature techniques, wake steering, has already shown in field tests to be a viable strategy for increasing the farm yield [10]. Aside from that purpose, the turbines could also provide grid ancillary services. Ref. [26] and Ref. [4] showed how to enable a wind farm to serve for secondary frequency regulation. Other authors have investigated how wind turbines could be enabled to closely follow a production set point, called power tracking [9, 33]. Finally, Refs. [30, 31, 14] show how online control algorithms can be used to reduce structural loads on turbines to ultimately reduce the LCOE.

One commonality for these (non comprehensive) examples of promising applications is that they all require ever more accurate predictions of the local turbine inflow conditions. Flow quantities at the rotor need to be estimated in real time, but also forecast in the short and medium term, as input for the control algorithms. For the effective design of a wake steering controller, it is e.g. important to consider the inherent wind direction variability [6]. Surrogate models, that describe the wind farm flow field, are therefore an integral part of any application. Often low computational cost is crucial which is why low fidelity engineering wake models are very popular [15, 2]. However, they fail at adequately capturing shorter time scales, as they describe by design a steady-state, long term average situation. In reality, changes in the flow propagate through the wind farm with a finite speed and do not affect all turbines simultaneously. Furthermore, wakes experience meandering movements. Consequently, the use of static wake models is becoming problematic when farm sizes increase and the time windows of interest

decrease. As both trends continue, this poses a limiting factor to the effectiveness of wind energy control applications.

To address this issue, a range of low to medium fidelity dynamic models, applicable to shorter time scales, have already been proposed. Most prominent is the dynamic wake meandering (DWM) model. It established the conjecture of the wake as a passive tracer, that is displaced by large scale eddies [18]. Recently, it has been further extended for atmospheric stability effects [16] and connected to load models in its FAST.Farm implementation [25]. In LIDAR campaigns the predicted wake center position matched well with the measurements [3, 29]. Further studies additionally tuned the wake advection and expansion rate [23, 20].

With lower fidelity, but still incorporating a time dimension, Ref. [11] proposed a dynamic extension of a static wake model. In the state-space FLORIDYN model, which is reimplemented in this paper, flow conditions propagate through wake observation points. The step-wise advancement in time models the wake movements and delay in ambient changes. A conventional wake model is used to calculate the velocity deficit at the discretized positions. The idea was extended with flow sensing turbine observers [19]. However, apart from that, the concept has not been widely tested. It is still to be investigated what niche the model can fill and for which time scales it can deliver useful predictions.

Despite the ongoing development, low- and mid-fidelity surrogate models will probably not be able to capture all relevant flow processes with sufficient accuracy in the near future. It makes therefore sense to use them in a closed-loop framework. E.g. in Ref. [8], the parameters of a dynamic surrogate model were adapted to changing ambient conditions with an online tuning algorithm. FLORIDYN was also already tested in combination with a Kalman filter [12]. However, the above mentioned studies were conducted in conjunction with LES simulation data or nacelle mounted LIDAR systems. Turbine SCADA data has not been used yet, however is often readily available. One reason for the lack of studies is that the data is usually averaged to 10 min intervals where most propagation effects are invisible. Recently, sites with higher resolution SCADA data sets became available. This opens the possibility to examine dynamic processes of the wind farm flow on shorter time scales. 1 Hz sampled data was for example used to calculate time delays in the power signal between turbine pairs in an offshore and onshore farm, respectively [24, 21].

This paper aims at the lack of studies with high frequency SCADA data and low-fidelity dynamic wake models. The focus is on a turbine pair interaction in an onshore wind farm. The first descriptive part investigates the time delay and level of coherence in the power signals of the two turbines. The second part describes the application of a FLORIDYN-like dynamic wake model for power prediction of the downstream turbine. As no LIDAR or mast measurements are available, the model input needs to be generated by the upstream turbine SCADA measurements. This requires adequate filter windows. To reveal possible design issues, the model is used in open loop configuration and the parameters are tuned offline. This approach is important before obscuring possible bad design decisions by a corrective online algorithm.

2. Methodology

2.1. Power signal cross-correlation

This section presents the methodology used to analyze propagation effects and time delays in the high frequency SCADA measurements. Throughout the paper, the analysis is performed on a selected turbine pair, denoted WT_A and WT_B. WT_A represents the unwaked upstream and WT_B the downstream turbine. The situation is shown for two subsequent points in time in Fig. 1. Power fluctuations will occur on both machines, raising the question if and how strongly they are correlated. The level and delay of the cross-correlation then allows to draw conclusions about propagation effects.

The produced power of WT_A, although subject to free stream, will fluctuate on the scale

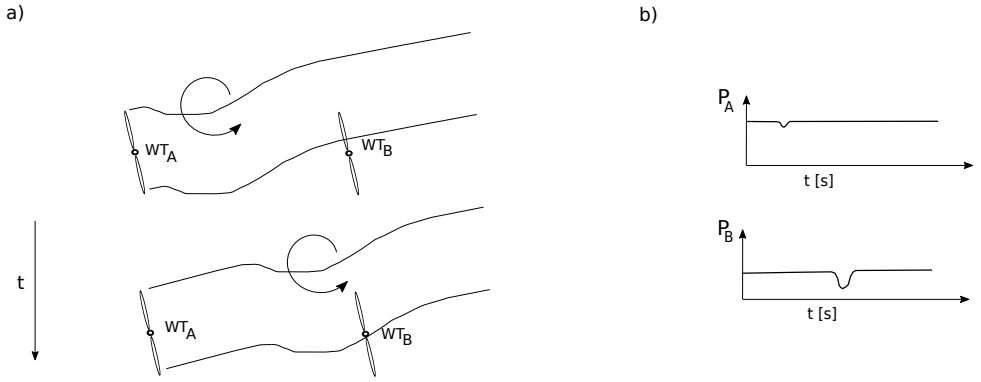

Figure 1. a) Idealized depiction of the propagation of a large eddy structure at two time instances. b) Power signal during the passage. The power of WT_A fluctuates when the eddy passes through the rotor, the fluctuation at turbine WT_B occurs later and is amplified by the wake of WT_A.

of seconds [28]. This is caused by variability in the inflow wind speed as well as direction changes. The responsible flow structures need to have a certain size, as the rotor area filters out small scale turbulence. Fig. 1 shows WT_B in a waked condition, i.e. both turbines are aligned with the mean flow ($WT_A \rightarrow WT_B$). According to Taylors frozen turbulence hypothesis, the downstream turbine will experience a similar ambient flow field after a time delay [27]. As depicted, a propagating turbulent structure caused a small power drop at turbine WT_A and is assumed constant over the transit distance. However, the situation is complicated by WT_A's generated wake, disturbing the ambient flow field. Following the conjecture of the DWM model, wake cross sections are displaced rigidly by large eddies. While these will propagate with the mean flow, the wake itself probably travels at a slower rate due to its velocity deficit. LIDAR experiments [3, 20] found indeed, that a slower advection speed better predicts the wake center position in the scans. Depending on the overlap upon impingement, the wake causes additional power drops and an increase of turbulence at WT_B. The mentioned effects will superimpose each other and it can be expected that the presence of the wake will influence the delay time and level of cross-correlation. If the downstream turbine WT_B is not in a waked condition, e.g. southern wind direction in the figure, the turbulent structures are probably not large enough to encompass both turbines. In that case, the cross-correlation of the two power signals is expected to be lower [24].

The evaluation of the cross-correlation in the available SCADA power signals (P_A, P_B) is similar to Ref. [24] as described in the following. The 1 Hz time series is first partitioned in intervals, with length T_I of continuous operation. The intervals need to be long enough to allow enough turbulent structures to propagate through both turbines. Yet short enough so that only small trends in wind speed or wind direction occur. Intervals, during which the turbines are yawing, are consequently omitted. All obtained intervals are then analyzed for cross-correlation of the two power signals. The first half of the interval of P_A is compared to an equal length, but time shifted, sub-interval of P_B. This ensures that the same amount of data is used for every

time shift. The covariance of the power signal of one sub-interval starting at time t_0 is

$$\mathrm{cov}(P_A, P_B(\tau)) = \frac{2}{T_I}\int_{t_0}^{t_0+T_I/2}(P_A(t)-\bar{P}_A)(P_B(t+\tau)-\bar{P}_B)\mathrm{d}t \ , \tag{1}$$

with τ [s] as the time delay. $\bar{P}_A$, $\bar{P}_B$ are the average power in the respective sub-interval. The correlation coefficient is obtained through normalization

$$r(\tau) = \frac{\mathrm{cov}(P_A, P_B(\tau))}{\sqrt{\mathrm{var}(P_A)\ \mathrm{var}(P_B(\tau))}} \tag{2}$$

with the variances of the power signals in the respective sub-interval. Eq. 2 is evaluated for a range of increasing time delays $\tau \in [0, T_I/2]$ s. If the described processes retain a part of the signal, the correlation will be maximum after a certain time has passed. This delay of maximum correlation is however dependent on the ambient wind speed. Therefore, as suggested by [24], τ is normalized

$$\tilde{\tau} = \tau\frac{\bar{U}_B(\tau)}{x_{AB}} \tag{3}$$

by the distance between the turbines x_{AB} and the average velocity measured at the downstream turbine $\bar{U}_B$. This allows for the aggregation of results from Eq. 2 from many data intervals.

2.2. Implementation of the dynamic wake model

The implementation of the dynamic wake model is for the most part analogous to the FLORIDYN proposal presented in Ref. [11]. The reader is referred to this original paper for a more detailed derivation. A short description that discusses the model for a single turbine and its wake is given in the following. The main idea is to propagate flow quantities through observation points (OPs) in a state space description. Figure 2 depicts the model for two consecutive states $k \to k+1$. Differently to Ref. [11], wake and ambient flow quantities are in the present implementation represented by two separate sets of OPs, represented in the figure with white and black markers.

Their positions in X-Y space (a horizontal plane at hub height) are

$$\mathbf{x}_w^k = \begin{bmatrix} x_{w,1} \\ x_{w,2} \\ \vdots \\ x_{w,Nw} \end{bmatrix}^k \quad \text{and} \quad \mathbf{x}_a^k = \begin{bmatrix} x_{a,1} \\ x_{a,2} \\ \vdots \\ x_{a,Na} \end{bmatrix}^k \tag{4}$$

for a number of N_w wake and N_a ambient OPs respectively. The latter explicitly represent the undisturbed background flow. The i-th ambient OP contains the ambient flow quantities wind speed $U_{a,i}$, wind direction Γ_i and turbulence intensity $I_{a,i}$. All currently present ambient quantities are contained in

$$\mathbf{U}_a^k, \mathbf{\Gamma}^k, \mathbf{I}_a^k \in \mathbb{R}^{N_a \times 1} \ . \tag{5}$$

Wake OPs on the other hand represent the bulk wake flow and define the wake center line. For that, each point contains firstly the delayed control inputs yaw misalignment γ_i and induction factor a_i, summarized as

$$\boldsymbol{\gamma}^k, \mathbf{a}^k \in \mathbb{R}^{N_w \times 1} \ . \tag{6}$$

Secondly, each wake OP represents a wake velocity deficit ΔU_i. Its magnitude and profile are calculated with a suitable wake model. In a LIDAR wake tracking experiment [29] was able to fit a bi-variate Gaussian profile on quasi-instantaneous snapshots. The wake deficit at each

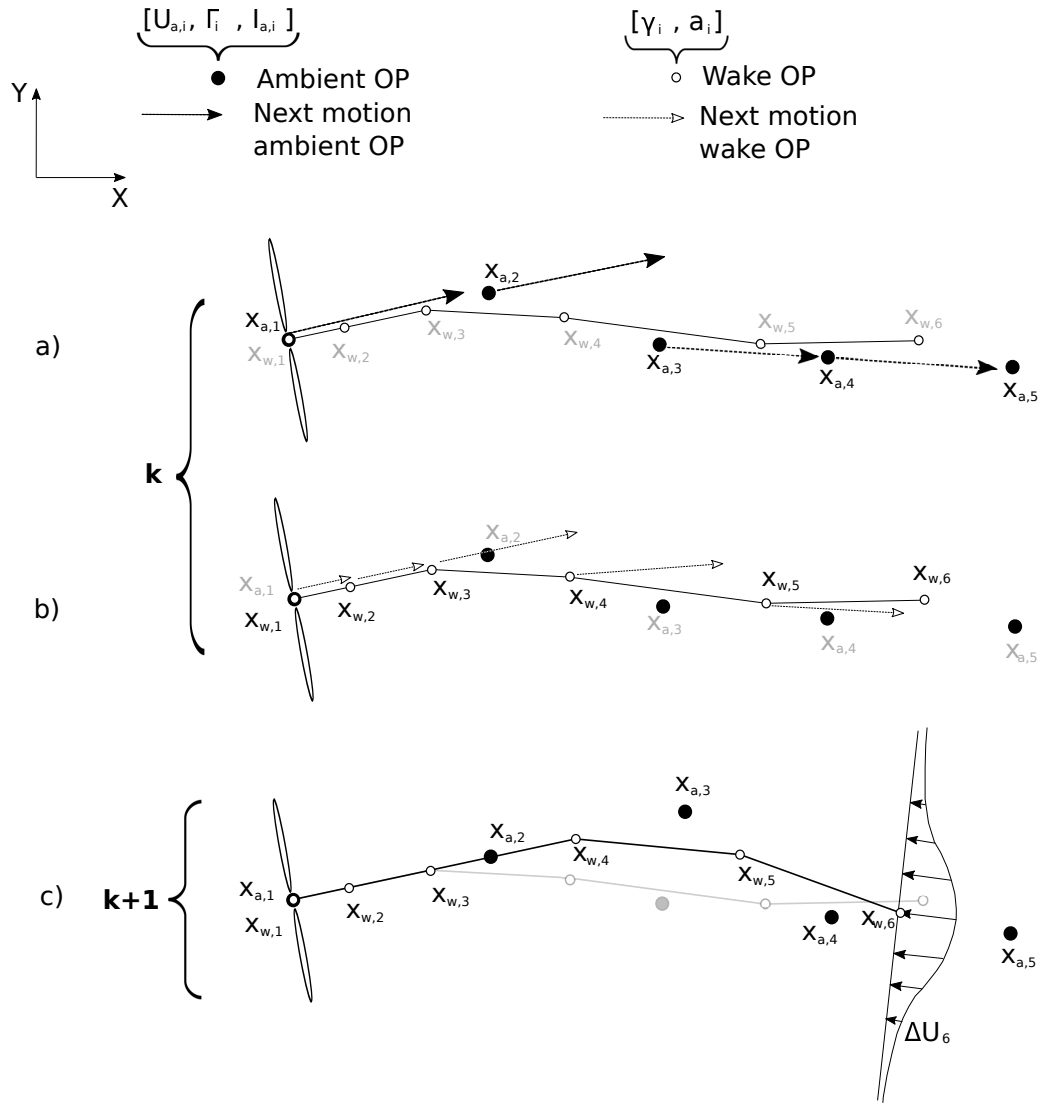

Figure 2. Dynamic wake model for a single turbine for two consecutive states $k \rightarrow k+1$. The arrows in subplot a) show the update direction for the ambient points at state k. Subplot b) shows the update direction for the wake OPs at state k. Subplot c) shows the new state after the locations have been updated at $k+1$. The ambient wind direction Γ_2 at $x^k_{a,2}$ causes a change in wake trajectory. One velocity deficit profile is shown at $x_{w,6}$.

wake OP is therefore calculated with the Gaussian wake model [2], as depicted in Fig 2c. The readily available FLORIS framework [22] was used for this task. For the calculation, the ambient conditions from the ambient OPs need to be first mapped to the wake OPs. This is done by linear interpolation $\mathbf{F}^k_a \rightarrow \mathbf{F}^k_w$, where $\mathbf{F}$ represents any of the ambient quantitites. The velocity deficit at the i-th wake OP can then be calculated with the delayed ambient conditions and control inputs

$$\Delta U^k_i(r) = f_w(r|x_{w,i}, U_{w,i}, I_{w,i}, \gamma_i, a_i)^k \ , \tag{7}$$

dependent on the radial coordinate from wake center r. The wake added turbulence $I_{add,i}$ is calculated in a similar manner with the model presented in reference [7].

The reason for two separate sets of OPs is to allow for a different propagation speed of wake

and ambient flow quantities. While changes in U_a or Γ propagate with mean undisturbed wind speed, the wake can move at slower rate. This is depicted by the two plots in Fig. 2ab that show the motion for the next update step. It can be seen that the environmental points are going to propagate a larger distance than the wake OPs. The advection speed of the wake, u_w, is obtained by subtracting the average velocity deficit from the ambient flow

$$u_{w,i}^k = U_{w,i}^k - \Delta\bar{U}_i^k = U_{w,i}^k - \frac{1}{A_w}\int_{A_w} \Delta U_i^k(r)\mathrm{d}A \ . \tag{8}$$

The wake area A_w is defined to extend until 99% of the ambient wind speed is reached. For the next time step, both kind of OP positions can now be updated according to

$$\mathbf{x}_w^{k+1} = \mathbf{A}\mathbf{x}_w^k + \mathbf{B}x_{w,1} + \mathbf{A}\mathbf{u}_w^k\Delta t \tag{9}$$

$$\mathbf{x}_a^{k+1} = \mathbf{A}\mathbf{x}_a^k + \mathbf{B}x_{a,1} + \mathbf{A}\mathbf{U}_a^k\Delta t \ . \tag{10}$$

The state and system matrices $\mathbf{A}$, $\mathbf{B}$ are defined as in Ref. [11]. Subsequently, the ambient quantities and control inputs are propagating to the next OP with

$$\mathbf{F}_a^{k+1} = \mathbf{A}\mathbf{F}_a^k + \mathbf{B}F_{a,1}^k \ , \tag{11}$$

similarly for the control inputs. The new model state is depicted in Fig. 2c.

New ambient conditions and control inputs enter the state space at the first OP located at the turbine rotor. If in free stream, the ambient conditions and control inputs can be provided as a feed e.g. from SCADA measurements. A waked condition is detected if external OPs are in the proximity of the rotor. In that case, firstly, ambient conditions are transferred to the waked turbine by inverse distance weighting $\mathbf{F}_{\mathrm{a,ext}} \rightarrow F_{a,1}$. Secondly, the effective impinging velocity deficit is mapped to the rotor through spatial interpolation $\Delta\mathbf{U}_{\mathrm{ext}} \rightarrow \Delta U_1$. The reduced inflow speed is then calculated through

$$U_{\mathrm{infl}} = U_{a,1} - \Delta U_1. \tag{12}$$

3. Site description

The site with the available data set consists of 12 × 2 MW machines. The rotor diameter is $D = 82$ m and the hub height 80 m. The terrain is characterized by gently rolling hills. Altitudes in a 3 km radius differ from ca. 150 m to 370 m above sea level. The turbine base heights vary from approximately 300 m to 360 m. The ground roughness is characterised by grassland with patches of low-lying bushes. Fig. 3 shows a close-up of the western part of the site. For highest wind direction frequency, the chosen turbine pair is located on the western edge. Both turbines are embedded in a north-south slope. The figure additionally shows a snapshot of wakes and the observation points, that make up the wake of WT_A.

24 month of 1 Hz data were available from 2019 to 2021. The channels included power, nacelle anemometer and wind vane measurements. To allow filtering and correcting, the data was first downsampled to 10 and 1 min. Then, the nacelle position signal was corrected. This was done firstly, by identifying sudden jumps and drifts through comparing individual yaw signals to the farm average. Secondly, by manually controlling the geometric wake impact directions. The rotor equivalent wind speed (REWS) was calculated using the manufacturer power curve in region II and binned pitch curve in region III. The density was calculated with temperature recordings and an air pressure time series from reanalysis data. The obtained corrections to the wind direction were reapplied to the high-frequency data and periods of outliers were removed.

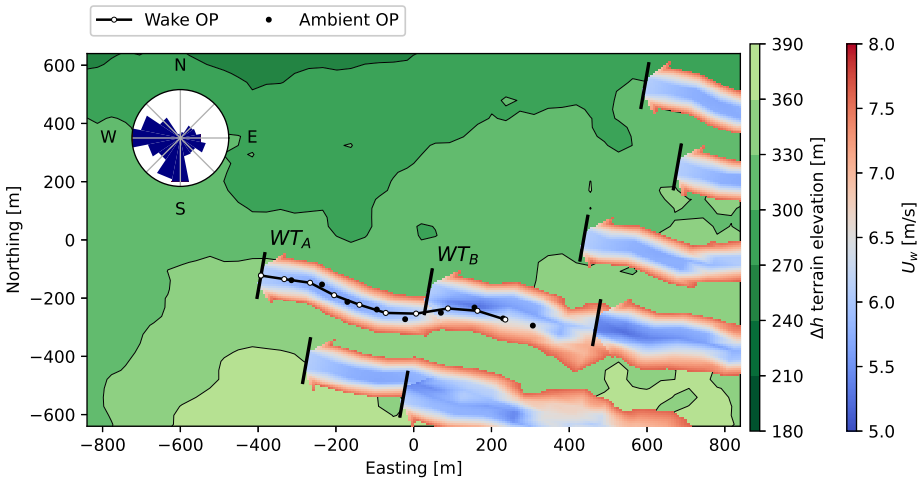

Figure 3. Close-up of the terrain of the western part of the wind farm. The investigated turbine pair is marked with WT_A and WT_B. A snapshot of emitted wakes is overlaid onto the terrain contour. Additionally depicted are the observation points that make up the wake of WT_A. The wind rose shows the wind direction frequency distribution.

4. Results

4.1. Cross-correlation analysis

Section 2.1 described the methodology for analysing the power signal cross-correlation for a turbine pair. This section presents the results for the selected two turbines in Fig. 3. The wind direction Γ was determined with the nacelle vane of WT_A. Geometrically, WT_A and WT_B are fully aligned for $\Gamma = 277°$. The analysis was therefore restricted to a sector of $\Gamma \in [265, 290]°$.

For partitioning the time series, the studies [21, 24] use an interval length of $T_I = 10$ min. This was followed in the present study which led to 961 usable intervals in the chosen sector, corresponding to 6.7 days of data. The behaviour of the correlation coefficient r with increasing delay was then calculated with Eq. 2 for all intervals. The turbines are separated by $x_{AB} = 434$ m. Undisturbed flow would need $\tau = 72$ and 43 s to reach WT_B at ambient speeds of 6 and 10 ms^{-1} respectively. This shows that the tested delay range of $\tau \in [0, 300]$ s is sufficient. Secondly, it highlights the necessity to normalize the time delay according to Eq. 3.

The main plot in Figure 4 shows the averaged $r(\tilde{\tau})$-lines binned in 5° sub sectors. The right subplots give an impression of the wake overlap situation of each sub sector. These plots were generated with a steady state wake model FLORIS [22]. Note that the investigated dynamic situations are not captured by this long-term average. The distribution of the cross-correlation lines firstly shows that the power signals are almost independent for $r(0) \approx 0.1$. With increasing time delay, the level of correlation peaks. This suggests that parts of the inflow signal are retained over the propagation to the downstream turbine. The maximum levels of 0.3-0.5 show however also, that a degree of randomness changes the inflow. The correlation levels are still higher than in Ref. [24]. This could be due to the much closer spacing compared to an offshore wind farm.

The peak of maximum correlation should occur at $\tilde{\tau} > 1$ if the most important fluctuations travel at the reduced speed of the wake. This is because, due to wake recovery, the normalization factor $\bar{U}_B(\tau)$ is probably an overestimation for a mean advection speed. For most of its path, the wake travels at a slower rate. The sub sectors with $\Gamma > 275°$ agree with this assumption. The peaks are however not very sharp, which could be due to the mentioned superposition with faster propagating ambient quantities. For the sub sectors $\Gamma < 275°$, the maximum correlation

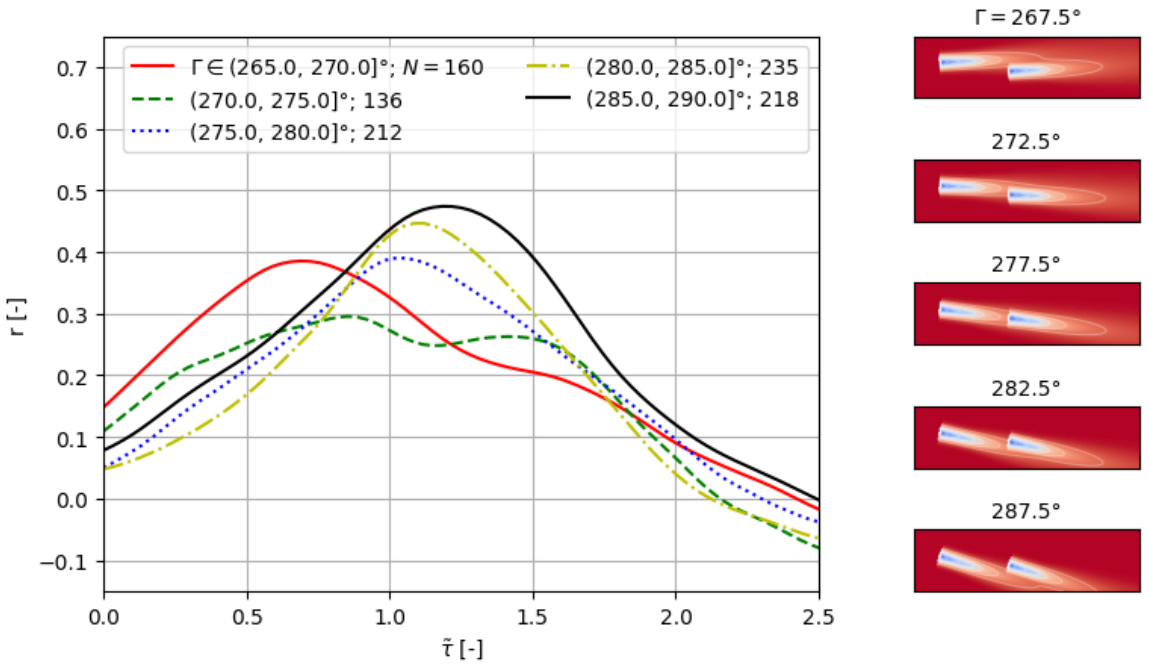

Figure 4. Averaged cross-correlation binned in 5° sub sectors with N number of intervals in bin. The time delay $\tilde{\tau}$ is normalized. The wake model plots on the right visualize the long-term average situation for the sub sectors.

occurs when $\tilde{\tau} < 1$ and there are even two peaks in the case of $\Gamma \in [270, 275]$. It is not clear what the ground reason for the unexpected early peak in these two sectors is. The downslope of the terrain could induce additional turbulent effects. Another reason could be the reduced amount of data, that is available from these directions. It can however be concluded that a time delay is present in all power signals. This motivates the use of a dynamic wake model.

4.2. Simulation with the dynamic wake model

The same set of intervals is now simulated with the dynamic wake model. For every 10 min interval, the model is set up as follows. A step of $\Delta t = 5$ s is used for advancing in time. The number of ambient and wake OPs is $N_a = N_w = 20$. Measurements from WT_A provide the model input for ambient wind speed and direction. The ambient turbulence and density were assumed constant as $I_a = 0.15$ and $\rho = 1.225$ kgm^{-3} respectively. The model predicts the effective inflow wind speed U_{infl} (Eq. 12) at WT_B to obtain the power production P_B. The first 100 s of every simulation are discarded in the post processing as the initial conditions need time to propagate to the downstream turbine. The model performance is assessed through the normalized error

$$\epsilon = \frac{P_B - P_{B,model}}{P_{\text{rated}}} \,, \tag{13}$$

and, additionally, through a correlation coefficient of the two signals

$$\rho = \frac{\text{cov}(P_{\text{B}}, P_{\text{B,model}})}{\sqrt{\text{var}(P_B)\ \text{var}(P_{\text{B,model}})}} \,. \tag{14}$$

The latter indicates if the modelled fluctuations agree with the measurements in time.

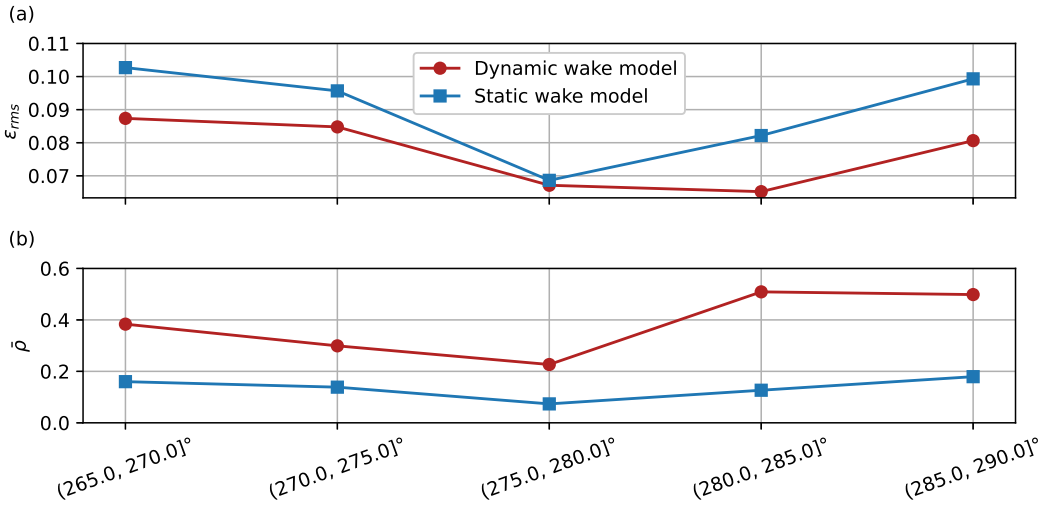

Figure 5. Directional model error (a) and average correlation (b) for the dynamic and static wake models.

An important question is, whether the nacelle wind vane of WT_A can be used to induce the correct meandering motions. As a point measurement, the vane is affected by smaller scale atmospheric fluctuations as well as turbulence generated by the rotor. According to the DWM conjecture, displacing eddies should have at least twice the diameter of the wake itself [18]. The suggested filter time window is therefore $T_f = 2D/U_a$. The application of this time scale to sonic anemometer measurements from a met mast for the same purpose showed convincing results [29]. With the present turbine, a 20 s moving average window for an ambient wind speed of 8 ms^{-1} would be required. The used nacelle instrumentation seems however too volatile so that the induced wake movements did not match the observed P_B. This is probably a result of the non-clean inflow of the wind vane. By increasing the averaging window to 4 D, the match improved considerably. For the given example, this results in a $T_f = 40$ s filter. As now only larger scale structures can be captured, the power and REWS signals were averaged as well. Since the rotor already acts as a spatial filter, these were filtered with with a shorter window of $T_f/2$.

The standard calibration of the utilized wake model (Eq. 7) describes a long-term average situation. It includes meandering movements, like shown in Fig. 1 and the velocity deficit is smeared out [5]. Likely, this is not an adequate tuning for the present purpose. The model is consequently recalibrated with a data subset of 40 intervals. An SLSQP algorithm was used to minimize the r.m.s. of Eq. 13 with respect to the wake expansion parameter, starting from $k_a = 0.38$. The tuning resulted in a value of $k_a^* = 0.05$, which is considerably smaller than the original. As expected, the wake becomes more focused.

Figure 5 shows the overall error ϵ_{rms} and the average correlation coefficient $\bar{\rho}$ for the tuned dynamic model for all intervals. The results are binned in the same sub-sectors as in Figure 4. A static Gaussian wake model, with similar tuning, is reported in the same figure for comparison. Contrary to the dynamic model, changes at WT_A take here immediate effect at WT_B. Throughout all sectors, the dynamic model provides an improvement of error and signal correlation. Interestingly, at full alignment, the difference in error is low. Likely, because the downstream turbine is fully waked most of the time, a prediction of the exact overlap is less critical here. In the slightly misaligned sectors, a delayed wake position seems to be more important. The improvements are better for $\Gamma > 280°$. This agrees with the findings in

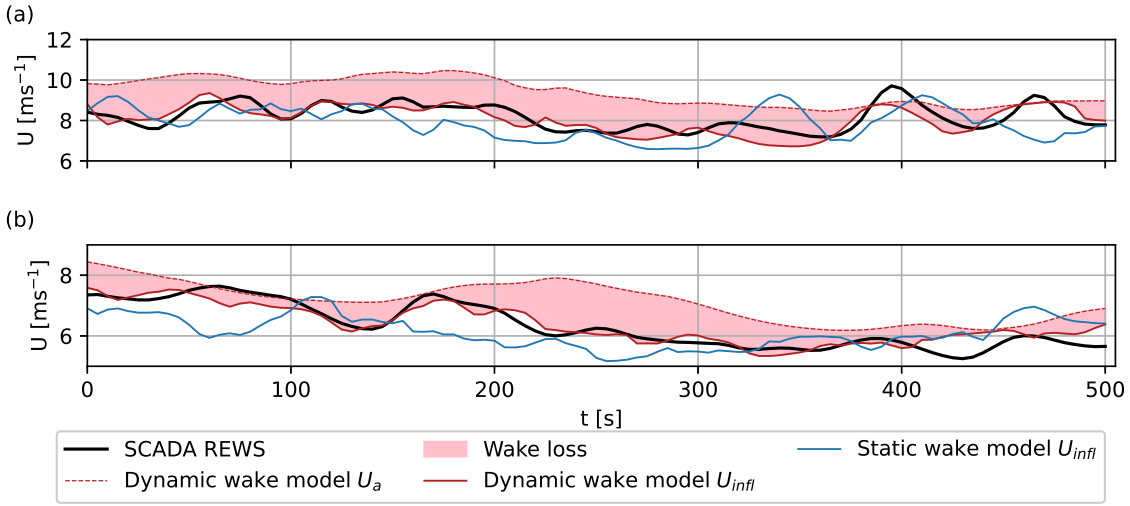

Figure 6. Measured and model-predicted REWS at WT_B, for two different time intervals. The prediction of a static, instantaneous wake model is given for comparison. Due to initialization time, the first 100 s of the 10 min interval have to be discarded. Additionally displayed are the dynamic predictions of ambient wind speed U_a and wake loss.

section 4.1 where the data cross-correlation level was higher for these sectors.

Finally, Figure 6 shows the measured as well as predicted inflow wind speed U_{infl} at WT_B for two example intervals. The static model is again reported for comparison. The dynamic model shows a reasonable agreement to drops and surges. The static model, on the other hand, predicts fluctuations prematurely. The plot additionally shows the estimation of ambient wind speed U_a at WT_B from the dynamic model. It is visible that the undisturbed wind speed changes on a slower scale than the wake losses.

5. Conclusion and outlook

The present study aimed to highlight the capabilities and limits of initializing an open-loop dynamic wake model purely with high frequency SCADA data. Results indicate, that delay effects must be accounted for when modelling shorter time scales. The presented low-fidelity dynamic wake model can capture filtered fluctuations. The error is reduced as well as correlation increased. Similar results were obtained by investigating other turbine pairs in the cluster. Reasons for deviations and possible improvements could be:

- The nacelle wind vane does not provide information on vertical fluctuations. Consequently, wake movements in vertical direction are missing in the model. Meandering in vertical direction is restricted by the ground, but can still have a considerable magnitude [13].
- Unmodelled terrain effects. As seen in section 2.1, the terrain probably has an affect on the wake propagation. This connects to the first point via possible ground reflections.
- The nacelle wind vane is affected by the rotor. More robust filter algorithms could improve the signal. Possibly using the wind direction information from surrounding turbines [1].
- Unmodelled influence of ambient conditions. This requires their estimation from the SCADA measurements.

The presented model provides a robust basis for an extension to multiple turbine interactions. The study suggests model limitations, which can be corrected by an online algorithm.

6. Acknowledgements

The authors express their gratitude to Mr. Benjamin Dittrich and Mr. David Coimbra from Energiekontor AG, who granted access to the field data and supported this work. The work has also been supported by the e-TWINS project (FKZ: 03EI6020A), which receives funding from the German Federal Ministry for Economic Affairs and Energy (BMWi)

References

[1] Jennifer Annoni et al. "Wind direction estimation using SCADA data with consensus-based optimization". In: *Wind Energy Science* 4.2 (2019).

[2] Majid Bastankhah and Fernando Porté-Agel. "A new analytical model for wind-turbine wakes". In: *Renewable energy* 70 (2014), pp. 116–123.

[3] Ferhat Bingöl, Jakob Mann, and Gunner C. Larsen. "Light detection and ranging measurements of wake dynamics part I: one-dimensional scanning". In: *Wind Energy* 13.1 (2010).

[4] S. Boersma et al. "A constrained wind farm controller providing secondary frequency regulation: An LES study". In: *Renewable Energy* 134 (2019).

[5] Robert Braunbehrens and Antonio Segalini. "A statistical model for wake meandering behind wind turbines". In: *Journal of Wind Engineering and Industrial Aerodynamics* 193 (2019), p. 103954.

[6] Filippo Campagnolo et al. "Wind tunnel testing of wake steering with dynamic wind direction changes". In: *Wind Energy Science* 5.4 (2020).

[7] A. Crespo and J. Hernandez. "Turbulence characteristics in wind-turbine wakes". In: *Journal of Wind Engineering and Industrial Aerodynamics* 61.1 (1996).

[8] Bart M. Doekemeijer et al. "Online model calibration for a simplified LES model in pursuit of real-time closed-loop wind farm control". In: *Wind Energy Science* 3.2 (2018).

[9] Paul Fleming et al. "Computational fluid dynamics simulation study of active power control in wind plants". In: *2016 American Control Conference (ACC)*. 2016 American Control Conference (ACC). IEEE, 2016.

[10] Paul Fleming et al. "Field test of wake steering at an offshore wind farm". In: *Wind Energy Science* 2.1 (2017).

[11] Pieter M O Gebraad and J W van Wingerden. "A Control-Oriented Dynamic Model for Wakes in Wind Plants". In: *Journal of Physics: Conference Series* 524 (2014).

[12] P.M.O. Gebraad, P.A. Fleming, and J.W. van Wingerden. "Wind turbine wake estimation and control using FLORIDyn, a control-oriented dynamic wind plant model". In: *2015 American Control Conference (ACC)*. 2015 American Control Conference (ACC). IEEE.

[13] J Jonkman et al. "Validation of FAST.Farm Against Large-Eddy Simulations". In: *Journal of Physics: Conference Series* 1037 (2018).

[14] S.K. Kanev, F.J. Savenije, and W.P. Engels. "Active wake control: An approach to optimize the lifetime operation of wind farms". In: *Wind Energy* 21.7 (2018).

[15] I Katic, Jørgen Højstrup, and Niels Otto Jensen. "A simple model for cluster efficiency". In: *European wind energy association conference and exhibition*. Vol. 1. 1986, pp. 407–410.

[16] Rolf-Erik Keck et al. "A consistent turbulence formulation for the dynamic wake meandering model in the atmospheric boundary layer". English. PhD thesis. Denmark, 2013.

[17] Torben Knudsen, Thomas Bak, and Mikael Svenstrup. "Survey of wind farm control-power and fatigue optimization: Survey of wind farm control". In: *Wind Energy* 18.8 ().

[18] Gunner C Larsen et al. "Wake meandering: a pragmatic approach". In: *Wind Energy: An International Journal for Progress and Applications in Wind Power Conversion Technology* 11.4 (2008), pp. 377–395.

[19] M Lejeune et al. "Data assimilation for the prediction of wake trajectories within wind farms". In: *Journal of Physics: Conference Series* 1618 (2020).

[20] E. Machefaux et al. "Empirical modeling of single-wake advection and expansion using full-scale pulsed lidar-based measurements". In: *Wind Energy* 18.12 (2015).

[21] S Macri et al. "Experimental analysis of time delays in wind turbine wake interactions". In: *Journal of Physics: Conference Series* 1618 (2020).

[22] NREL. *FLORIS. Version 2.4*. 2021.

[23] Inga Reinwardt et al. "Dynamic wake meandering model calibration using nacelle-mounted lidar systems". In: *Wind Energy Science* 5.2 (2020).

[24] Janna Kristina Seifert et al. "Correlations of power output fluctuations in an offshore wind farm using high-resolution SCADA data". In: *Wind Energy Science* 6.4 (2021), pp. 997–1014.

[25] Kelsey Shaler and Jason Jonkman. "FAST.Farm development and validation of structural load prediction against large eddy simulations". In: *Wind Energy* (2020).

[26] Carl R. Shapiro et al. "Model based receding horizon control of wind farms for secondary frequency regulation". In: *Wind Energy* 20.7 (2017).

[27] Geoffrey Ingram Taylor. "The spectrum of turbulence". In: *Proceedings of the Royal Society of London. Series A-Mathematical and Physical Sciences* 164.919 (1938), pp. 476–490.

[28] N Tobin, H Zhu, and LP Chamorro. "Spectral behaviour of the turbulence-driven power fluctuations of wind turbines". In: *Journal of Turbulence* 16.9 (2015), pp. 832–846.

[29] Juan-Jose Trujillo et al. "Light detection and ranging measurements of wake dynamics. Part II: two-dimensional scanning". In: *Wind Energy* 14.1 (2011).

[30] Mehdi Vali et al. "Adjoint-based model predictive control of wind farms: Beyond the quasi steady-state power maximization." In: *IFAC-PapersOnLine* 50.1 (2017).

[31] Mehdi Vali et al. "An active power control approach for wake-induced load alleviation in a fully developed wind farm boundary layer". In: *Wind Energy Science* 4.1 (2019).

[32] J. W. van Wingerden et al. "Expert Elicitation on Wind Farm Control". In: *Journal of Physics: Conference Series* 1618.2 (2020).

[33] Jan-Willem van Wingerden et al. "Active Power Control of Waked Wind Farms". In: *IFAC-PapersOnLine* 50.1 (2017).